Hindawi Publishing Corporation
International Journal of Navigation and Observation
Volume 2008, Article ID 426267, 11 pages
doi:10.1155/2008/426267

Research Article

Scattering-Based Model of the SAR Signatures of Complex Targets for Classification Applications

Gerard Margarit and Jordi J. Mallorqui

Remote Sensing Laboratory, Department Signal Theory and Communications, Universitat Politècnica de Catalunya, Jordi Girona 1-3, 08034 Barcelona, Spain

Correspondence should be addressed to Jordi J. Mallorqui, mallorqui@tsc.upc.edu

Received 5 February 2008; Accepted 14 May 2008

Recommended by Simon Watts

The modeling of complex target response in SAR imagery is the main subject of this paper. The analysis of a large database of SAR images with polarimetric and interferometric capabilities is used to accurately establish how the different structural parts of targets interact with the incident signal. This allows to relate the reflectivity information provided by SAR images with specific geometries and to fix variation reflectivity patterns in terms of different imaging parameters such as image resolution, incidence angle, or operating frequency. Most of the used images have been obtained from the SAR simulator of complex targets developed at UPC, which is able to generate realistic data for a wide range of observation and environmental conditions. The result is a precise scattering-based SAR model that opens the door, among others, to an alternative way for reliable geometry retrieval. Under this approach, a novel SAR classification method for ships has been proposed. The preliminary evaluation in simulated scenarios shows a notable classification capability even under strong clutter and ship motion conditions. Due to these promising results, the same methodology is intended to be applied to urban areas. Concerns about possible model limitations and required improvements are preliminarily treated.

1. INTRODUCTION

The proliferation of new SAR sensors with improved capabilities in terms of system resolution and information channels (polarimetry and interferometry) has increased the range of products that can be obtained from SAR imagery [1]. Examples are characterization and classification of man-made structures like ships or urban targets [2–5]. In the past, the limitations of sensors' performance have made it almost impossible to precisely retrieve those physical and geometrical parameters related with the imaged targets. This trend is currently changing with the new generation of airborne and orbital sensors.

Now, real data have higher diversity, as polarimetric channels are available, and increased revisiting times. Their adequate interpretation requires the development of new models, where the SAR signatures of complex targets become related with their geometries. The development of such models with real imagery is difficult and arduous because the required amount of data with the related ground-truth is not always available and can be too expensive to generate. A feasible alternative lies in the usage of realistic simulators, where flexibility and reduced cost can overcome previous limitations allowing to rapidly increase the knowledge in target scattering.

In this context, the current paper provides a new methodology for modeling the response of complex targets in SAR imagery based on the analysis of large stacks of simulated scattering maps [6]. By using an accurate and realistic SAR simulator, the response of each structural part of a target can be described in terms of the three-dimensional position, the scattering properties (reflectivity intensity and polarimetric behavior), and the dependence of these properties with respect to key imaging parameters (incidence angle and target orientation, resolution, operating frequency, etc.). All this information can help to predict the expected real SAR response for a given set of observation conditions and, hence, geometrical and physical information may be retrieved by simply inverting the relations established within simulation environments. As a result, a new target

model emerges, which can be exploited in a large number of applications.

The previous modeling methodology has been applied to ships [7] and urban targets [8]. This has been done with GRECOSAR [9], a simulator able to realistically simulate SAR images of complex targets within flexible and controlled scenarios. It works with 3D high-frequency ElectroMagnetic (EM) calculations using physical optics (PO) and physical theory of diffraction (PTD) [10, 11]. In a first step, a large number of fully polarimetric scattering maps (inverse SAR, ISAR) with resolution around centimeters have been used to study the dispersion behavior of targets in terms of their geometries and observation conditions. This has allowed to observe a specific scattering pattern from which the dispersion information can be linked with target geometry for a large range of views. In a second step, the signatures of targets have been analyzed in simulated SAR images. For an adequate image resolution, it follows that the previous scattering patterns can be related with the observed structures or, in other words, targets' geometry can be inferred from the scattering patterns.

As a result, the proposed scattering-based model of complex targets appears to be feasible for practical applications. Its usefulness in real scenarios has been evaluated by testing its potentialities for basing new classification/identification approaches. Special attention is placed on ships where the availability of robust algorithms is mandatory for complementing new ship monitoring techniques devoted to SAR platforms (see European IMPAST [12], DECLIMS [13], and LIMES [14] projects). In this sense, the vessel classification algorithm (VCA) working with polarimetric interferometric SAR (PolInSAR) imagery is presented [6]. Its operating principle is briefly described and some tests are carried out within simulated scenarios for the analyzed real-like observation conditions. The results show notable classification ratios even under adverse observation conditions, mainly manifested by sea clutter and ship motions [7]. Regarding urban environments, the conclusions derived from the model are used to improve real-data interpretation and the performance of interferometric-related applications such as subsidence.

This paper is structured as follows. Section 2 describes the modeling methodology stressing its advantages and limitations with respect to classical approaches. Section 3 presents samples of the scattering maps used to relate the model scattering behavior with its geometry. The reliability of the derived scattering patterns in SAR images is assessed in Section 4. They are exploited in Section 5, where the VCA algorithm and new guidelines for helping to improve the interpretation of urban data are introduced.

2. MODELING METHODOLOGY

Modeling the dispersion response of complex targets should take into account what follows: (1) the measuring variables (*model inputs*, i.e., polarimetric and interferometric data), (2) the parameters to be inverted (*model outputs*), and (3) the main application for which target modeling is sought. In our context, complex target modeling is conceived for characterization and classification and, hence, the retrieval of key geometrical information is the main goal (*model output*). To successfully do this process, accurate geometry-scattering relations are mandatory so that the reflectivity information of SAR images can be connected with specific geometrical shapes. For such purpose, large datasets have to be analyzed for the largest possible scenario diversity. In real scenarios, this task is extremely complex as, besides the long and costly measurement campaigns, the coordination between the sensor and testing scenarios should be almost perfect for reaching the planned observation conditions and acquiring accurate ground-truth. In most situations, for instance, with vessels at sea, this is almost impossible.

Recent works have suggested the possibility to exploit numerical tools for carrying out, in a first stage, the previous studies [7, 9]. Simulation presents two advantages: (1) the capability to quickly process a wide range of scenarios for which target models can be developed, and (2) the possibility to plan measurement campaigns, where observation conditions allow to efficiently test, improve, and/or validate the proposed model. The combination of both can lead to better models.

In this study, simulated images have been used. They have been obtained from the GRECOSAR numerical tool [9], which is able to reproduce in simple PC realistic SAR images of complex targets. It is based on UPC's GRaphical Electromagnetic COmputing (GRECO) solver [10] that estimates, for each single frequency, the radar cross-section (RCS) of 3D targets via high-frequency methods (PO, PTD). Targets are modeled with the CAD package GiD of the International Center of Numerical Methods for Engineering (CIMNE) [15]. Computer efficiency and scenario flexibility are the main advantages of the simulator. This allows to simulate any sensor for any operating band, mode, and resolution with polarimetric and/or interferometric capabilities. Target environment is configurable with dielectric materials, relative sensor-to-target orientation, incidence angle, and, in the case of vessels, speed, motion dynamics, and dynamic sea surfaces [16, 17]. Exhaustive tests performed with both canonical and complex targets have validated the code. Its potentialities for complex target studies have been shown in previous works devoted to ships [6, 7].

2.1. Model outputs

For classification applications, the parameters to be inverted have to be related with target's geometry. It would be desirable to obtain from data the three-dimensional position of all points defining the structure. However, this is not possible with radars as only a reduced group of geometrical shapes with high RCS is present in the image [2, 7, 18]. The remaining scatterers are either cluttered by the stronger ones due to the limited system resolution or have an RCS below the noise floor.

In this framework, the model is focused to find the 3D position of a set of significant scatterers that summarize the macroscale geometry of the different types of targets, like those obtained from polarimetric decompositions. Such scatterers are termed as *permanent polarimetric*

scatterers (PePSs) in the sense that they present similar scattering properties within a wide range of observation conditions. For each target model, particular combinations of PePSs are selected according to the analysis of simulated scattering maps derived for different observation conditions. Mathematically, the feature vector for target j can be denoted by

$$\Theta^j = \{\Theta_i^j\} \quad \text{for } 1 < i < N_{\text{PePS}}, \tag{1}$$

where N_{PePS} points to the number of PePSs for that target and

$$\Theta_i^j = \{a_i, \text{gr}_i, h_i, p_i\}^j \tag{2}$$

gathers the azimuth (a_i) and ground-range (gr_i) locations of scatter i, jointly with its height (h_i) and related scattering mechanism (p_i). *Scattering mechanisms* are defined according to the basic Pauli mechanisms [19], namely, "trihedral" for those mechanisms with odd number of reflections (sphere, flat planes, 3D corners, etc.), "dihedral" for those mechanisms with even number of reflections (2D corners), and "antisymmetric" for those mechanisms without the symmetry property. All three follow the orthogonality property and have appeared to be indispensable for increasing the discrimination capability among different PePS configurations [6]. This explains the importance of the polarimetric term p_i in (2). Other polarimetric decompositions could also be used, but orthogonality helps to better discriminate the interferometric phase information related to each mechanism.

2.2. Model inputs

The retrieval of the previous information needs from *polarimetric interferometric SAR* (PolInSAR) imagery. Certainly, SAR imagery provides information about azimuth (a_i) and ground-range (gr_i) scatter locations, SAR interferometry (InSAR) [20] about the relative height among scatterers (h_i), and, finally, SAR polarimetry (PolSAR) [19, 21, 22] about the associated scattering mechanisms (p_i). These relations are valid if each resolution cell does not contain more than one PePS with the same scattering mechanism. This implies that (1) it is possible to discriminate a maximum of three scatterers with different scattering mechanisms within the same resolution cell, and (2) a minimum of resolution is required for an adequate PePS discrimination. Different tests have shown that a resolution around 3 m seems to be enough for ship classification applications [6, 7].

The sensor requirements that imply the usage of PolInSAR with high resolution are quite demanding [17]. Certainly, the management of six information channels in the time slot of one synthetic aperture position increases the hardware complexity and, even worst, imposes important restrictions on the coverage (swath is severely limited if compared with single-pol SAR). By now, this can only be assumed by airborne sensors, despite the fact that the new operating modes of TerraSAR-X and Radarsat-2 are close to this goal if single-pass interferometry is not considered. In order to make an efficient usage of the available information, some alternatives are now under consideration, such as *alternate polarimetric* (AP) modes or *partial polarimetry* (PP) [23–25]. They allow to reduce the number of polarimetric channels but at the expense of some model approximations that in some cases cannot be applied, as in the case of ships against strong clutter conditions [17].

2.3. Modeling scheme

The scheme of the adopted modeling methodology can be summarized in the following points.

(i) Select a set of targets that can be considered as representatives of the different types that can be found.

(ii) Generate a large number of scattering maps with numerical tools that help to fix the scattering behavior of the different parts of targets' structure. These data have to be derived for a particular set of observation conditions (Φ^k) and should evaluate the impact of the surrounding environment. In a first approach, Φ^k is defined for the incidence angle ($\phi[^\circ]$), relative target-to-sensor orientation ($\beta[^\circ]$), and operating frequency (f[Ghz]) taking different values within a fixed range.

(iii) For a given set of observation conditions $\Phi^k = \{\phi, \beta, f\}^k$, define a particular feature set Θ^j for the type of target j. PePSs are selected by those scatterers presenting an RCS 10 dB higher than that of the surrounding scatterers and a stable polarimetric behavior within a solid angle of at least $\pi/3$ steradian (this is the solid angle subtended by a cone of 30° of aperture). Three issues are important in this definition: (1) stable polarimetric behavior for PePS i means to take the same value of p_i^j within the selected aspect angle (see (4) and (5)); (2) PePS 3D positions are expressed with respect to a local coordinate system within the target from which the migration to SAR location parameters (a_i^j and gr_i^j) is performed according to the particular imaging geometry (see Figure 1); (3) the threshold in the angular aperture is selected by the response of typical canonical scatterers, like trihedrals and dihedrals. This implies that the modeling methodology is focused to locate those structures with the closest scattering behavior to canonical targets.

2.4. Inversion scheme

Model inversion implies basically to retrieve the information of Θ_i^j for all the potential candidates of PePS. It assumes that target signature has been previously isolated from the environment with any of the currently available detection methods (see [26, 27] for ships and [5, 28, 29] for urban areas). In a first iteration, all local maxima present in target's signature for all polarimetric channels are selected (N_{lm}) (see Section 5.1). For each one, $\langle\Theta_n^j\rangle$ is estimated according to (1)

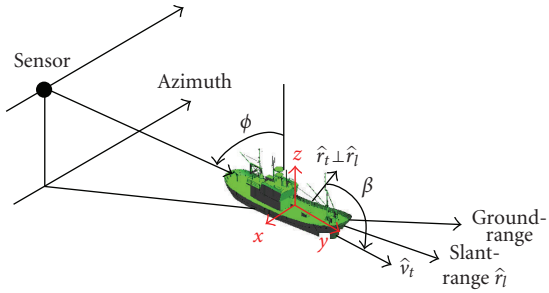

Figure 1: Local coordinate system used to define PePS within targets. The center is located at target's center of mass.

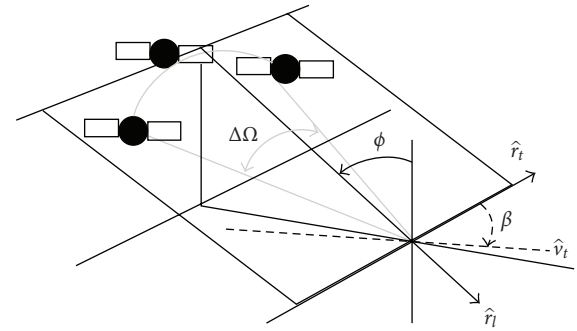

Figure 2: ISAR imaging geometry of GRECOSAR.

with $1 < n < N_{\text{lm}}$. The formulae required for this process are listed as follows. Regarding height,

$$\langle h_n^j \rangle = \sin\phi \left[\frac{cr_o}{4\pi f B^{\perp}} \Delta\psi - \frac{\Delta r}{\tan\phi} \right], \tag{3}$$

where $\Delta\psi$ and Δr fix the interferometric phase and slant-range difference of scatter n with respect to a fixed reference. r_o is the range, and $B^{\perp}$ is the perpendicular baseline, both known as radar parameters [20, 30]. Interferometric phase corresponds to the phase of the pixel of the interferogram related to scatter n. The interferogram is built by multiplying the master image with the complex conjugate of the slave for a particular polarimetric channel [20].

The polarimetric term p_i is estimated according to the significance of the Pauli scattering mechanism associated with the analyzed scatter n. This implies the following relations:

$$\begin{aligned}
\langle p_n^j \rangle &= 0 \quad \text{if } |p_{n,0}^j| > |p_{n,1}^j|, |p_{n,2}^j|, \\
\langle p_n^j \rangle &= 1 \quad \text{if } |p_{n,1}^j| > |p_{n,0}^j|, |p_{n,2}^j|, \\
\langle p_n^j \rangle &= 2 \quad \text{if } |p_{n,2}^j| > |p_{n,0}^j|, |p_{n,1}^j|,
\end{aligned} \tag{4}$$

where $|p_{n,xx}^j| = p_{n,xx}^j / \max\{p_{n,0}^j, p_{n,1}^j, p_{n,2}^j\}$ defines the normalized significance of the three Pauli mechanisms:

$$\begin{aligned}
p_{n,0}^j &= \frac{1}{\sqrt{2}} \frac{S_{hh}^n + S_{vv}^n}{2}, \\
p_{n,1}^j &= \frac{1}{\sqrt{2}} \frac{S_{hh}^n - S_{vv}^n}{2}, \\
p_{n,2}^j &= \frac{1}{\sqrt{2}} S_{hv}^n
\end{aligned} \tag{5}$$

for the elements of the monostatic master scattering matrix $[S]^n$ measured in the pixel of scatter n:

$$[S]^n = \begin{bmatrix} S_{hh} & S_{hv} \\ S_{hv} & S_{vv} \end{bmatrix}^n. \tag{6}$$

The term $xx = \{0, 1, 2\}$ is related to the "trihedral," "dihedral," and "antisymmetric" Pauli mechanisms. Finally, azimuth and ground-range locations are obtained from the azimuth ($a_{n,\text{SAR}}^j$) and slant-range ($\text{sr}_{n,\text{SAR}}^j$) positions of scatter n in the SAR image:

$$\begin{aligned}
\langle a_n^j \rangle &= a_{n,\text{SAR}}^j, \\
\langle \text{gr}_n^j \rangle &= \frac{\text{sr}_{n,\text{SAR}}^j + \langle h_n^j \rangle \cos\phi}{\sin\phi}.
\end{aligned} \tag{7}$$

The inversion process ends by selecting those PePSs whose combination better matches the list defined by Θ^j.

3. SCATTERING MAPS

The modeling methodology starts with the generation of stacks of scattering maps (Ω_j^k) defined for particular sets of observation conditions (Φ^k) and targets' types (j). This step has been done with GRECOSAR following the inverse SAR imaging geometry shown in Figure 2. Some samples are presented in this section for two different classes of targets: ships and buildings. The intrinsic geometries of both raise some particular scattering properties that can help to make the modeling process more efficient. For instance, the symmetric distribution of scatters in the normal direction to the line of sight (LOS) [18] induces a higher scattering stability within a wide range of views, and allows to use a unique feature vector (Θ^j) for characterizing the target. This normally happens with symmetric targets like ships, which appear to be specially suited for the modeling methodology [7, 16].

All the presented scattering maps are fully polarimetric and depict the normalized Pauli significance ($|p_{n,xx}^j|$) with an RGB-based color code: red→$|p_{n,0}^j|$ (first Pauli mechanism), green→$|p_{n,1}^j|$ (second Pauli mechanism), and blue→$|p_{n,2}^j|$ (third Pauli mechanism). They show the most representative cases of all those generated (see [6] for further details).

3.1. Modeling ship responses

Figure 3 provides scattering maps at X, C, and L bands for an incidence angle of $\phi = 20^\circ$ and three different target orientations, $\beta = \{295, 315, 335\}^\circ$. Three types of ships have been considered: a Spanish fishing vessel of 30 m long and 7 m wide (target $j = S0$), an Icelandic fishing vessel of 70 m long and 15 m wide (target $j = S1$), and a passenger ferry

Table 1: Feature vectors for targets $j = S0$, $j = S1$, and $j = S2$ and $\Phi^{SO1} = \{10-30^\circ, 280-350^\circ, 5.3-9.65\,\text{GHz}\}^{SO1}$. Heights ($z$) are normalized with respect to the lowest value in order to match interferometric height conventions.

Θ^{S0}					Θ^{S1}				
Θ_i^{S0}	x_i	y_i	z_i	p_i	Θ_i^{S1}	x_i	y_i	h_i	p_i
1	3.5	−10	0	0	1	3	−2	0	1
2	3.5	−5	0	0	2	−6	−14	6.5	1
3	−0.5	−8	2.5	1	3	−1	1	6.5	1
4	−0.5	−2	4.5	1	—	—	—	—	—
Θ^{S2}							—		
Θ_i^{S2}	x_i	y_i	z_i	p_i			—		
1	12	−25	0	0			—		
2	10	−25	0.5	1			—		
3	9	8	2.5	1			—		
4	9	−8	2.5	1			—		

Table 2: Feature vectors for $\Phi^{UO1} = \{20^\circ, 190^\circ, 9.65\,\text{GHz}\}^{SO1}$ and targets $j = U0$ and $j = U1$. Heights (z) are normalized with respect to the lowest value in order to match interferometric height conventions.

Θ^{U0}					Θ^{U1}				
Θ_i^{U0}	x_i	y_i	z_i	p_i	Θ_i^{U1}	x_i	y_i	h_i	p_i
1	−8	2	5.5	0	1	−4	2	0	0
2	−7	−3	2.2	0	2	4	−8	9.5	0
3	−6	−8	0	0	3	8	−1	12.5	0

of 200 m long and 30 m wide (target $j = S2$). As observed, each type of ship presents a particular distribution of strong scatters, PePS candidates, which appear to be stable within a specific range of views.

The selection criteria described in Section 2.3 have been applied to these datasets and have confirmed that each ship presents different PePS combination that leads to the feature vectors summarized in Table 1. They mainly correspond to dihedral interactions of cylindric structures (like masts and funnels) and trihedral behaviors due to corner geometries (like buttresses). Such vectors are valid for the set of simulated observation conditions $\Phi^{SO1} = \{10-30^\circ, 280-350^\circ, 5.3-9.65\,\text{GHz}\}^{SO1}$ that cover different range of values for incidence, target orientation, and operating frequency. The margin of validity in terms of incidence angle and target orientation is notably large and opens the door for characterizing a vessel with a reduced set of feature vectors. In Table 1, PePS 3D positions are expressed in the local coordinate system shown in Figure 3, from which SAR location parameters are derived according to the incidence and target orientation angles. Such conversion needs the knowledge of vessels' bearing that can be extracted from any of the currently available methods [31, 32]. Note also in Table 1 that the defined PePSs are valid for the complementary range of orientation values owned to the symmetry of the vessels' structure.

3.2. Modeling urban responses

The same procedure is now being conducted for urban areas. The presented results should be considered preliminarily as the work is still in progress and the amount of simulated images is not comparable with that currently available for ships. In this sense, Figure 4 presents some scattering maps similar to those introduced previously, but related to two different classes of buildings ($j = U0$ for the upper one and $j = U1$ for the lower one). The structures of both buildings are clearly depicted in Figure 6. They correspond to two structures within a test site, where ground-based SAR (GB-SAR) measurements were carried out by UPC [33, 34]. This has provided accurate ground-truth about building structure as well as external elements that may interfere. The images have been obtained for $\phi = 60^\circ$ and $\beta = \{190, 200\}^\circ$ at X band in order to reproduce the observation conditions of the GB-SAR sensor.

In the light of the obtained results, it follows that the response of these targets can be also described by a set of PePSs. The related feature vectors are summarized in Table 2 for which point positions are expressed in terms of the coordinate system depicted in Figure 4. Such scatterers are mainly related to frame points located in doors and windows (trihedral) and punctual wall-street interactions (dihedral). But now the scattering maps are not as stable as those obtained from vessels. In general terms, the whole response is appreciably modified (even by eye inspection) from one orientation to another, despite the fact that some particular PePSs can still be identified. The causes are the extremely complex environments that make most of the details to be able to contribute to the scattering map depending on the incidence conditions.

Therefore, it appears that building discrimination via target scattering is more difficult as the number of feature vectors demanded for covering target dispersion increases notably. However, due to the high realism achieved by GRECOSAR in reproducing the scattering information of real scenarios [8], other areas can take profit of these results. Examples may be the development of differential interferometry- (DInSAR-) related applications for subsidence monitoring [5] and the inclusion of polarimetric data provided by the new sensors, like TerraSAR-X or Radarsat-2.

4. MODEL ANALYSIS IN SAR IMAGES

This section tests the performance of the first model version generated in the previous section for SAR images. For such purpose, some of the previous simulations have been rerun for the SAR imaging geometry of Figure 1. A PolInSAR X band sensor covering the previously indicated incidences and providing a resolution of 2.3 m in azimuth and 1.3 m in range has been used.

4.1. Ship targets

Some ship samples are presented first in Figure 5 by expressing the significance of each Pauli mechanism in gray scale. The scenario does not take target environment into account

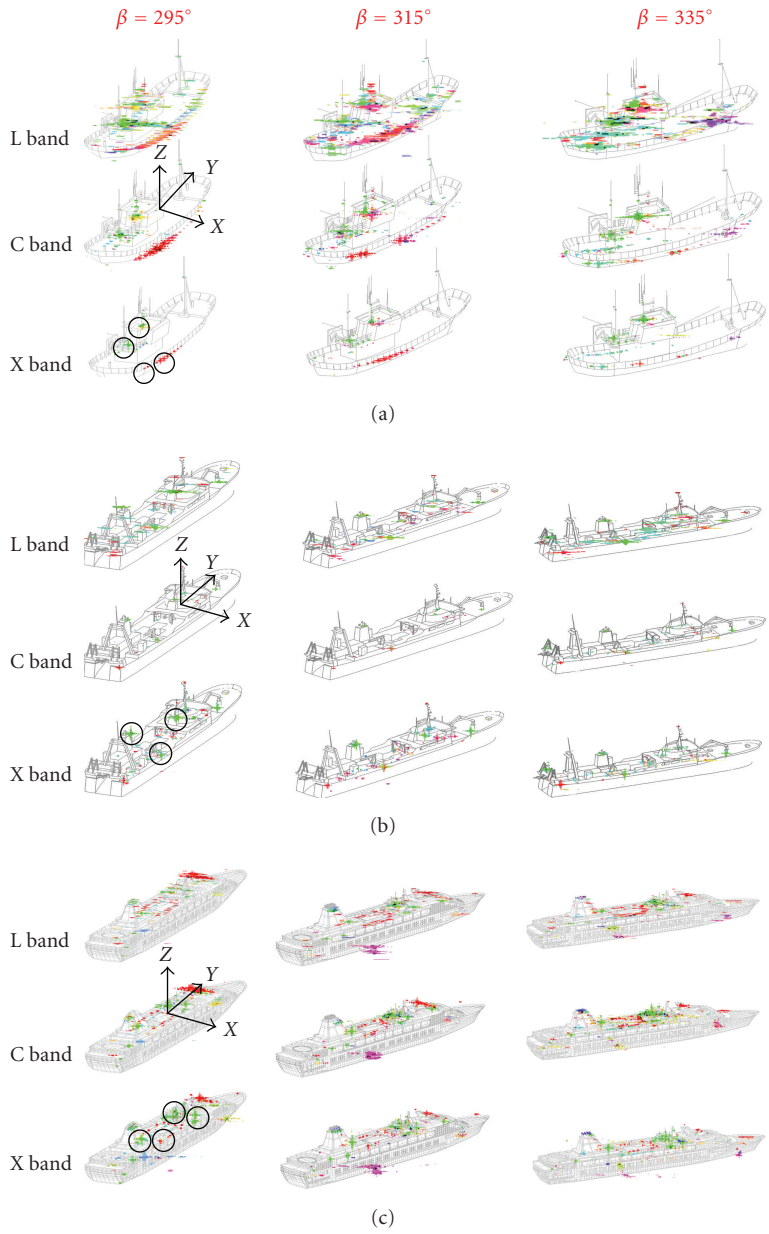

Figure 3: Scattering maps obtained for the SPA (a), ICE (b), and FER (c) vessels at L, C, and X bands with $\beta \in \{295, 315, 335\}^\circ$ and $\phi = 20^\circ$. They have been analyzed with the Pauli CTD theorem for a dynamic range of 25 dB. The lengths of the SPA, ICE, and FER ships are 30, 70, and 200 meters. Circles isolate the PePSs used in the feature vectors of Table 1.

so that qualitative data interpretation can be done. From all the contemplated bearings ($\beta = [295 : 10 : 355]$), Figure 5 only presents two of them, $\beta = 295, 315^\circ$ ($\phi = 20^\circ$), which can be considered as representatives of the remaining ones.

The inspection of these images shows that the isolation of those PePSs conforming the feature vectors is possible. They are imaged with the same scattering properties found in the scattering maps relative to polarimetric behavior, RCS, and spatial distribution. This implies that the proposed model can be inverted and, thus, valuable geometrical information is retrieved. In fact, this process has been done following the explanation of Section 2.4 and a confidence estimation of around 80% has been found.

However, the previous case is ideal and, normally, real scenes do not present such level of isolation between sea clutter and target response. Their interaction is higher and this leads to image corruption that can put PePS isolation at risk [7, 17]. Next section will further treat this point showing that a proper image post-processing can assure reliable model inversion even under adverse observation conditions.

4.2. Urban targets

Something similar has been done for the two building targets. In this case, PePS analysis is not performed while

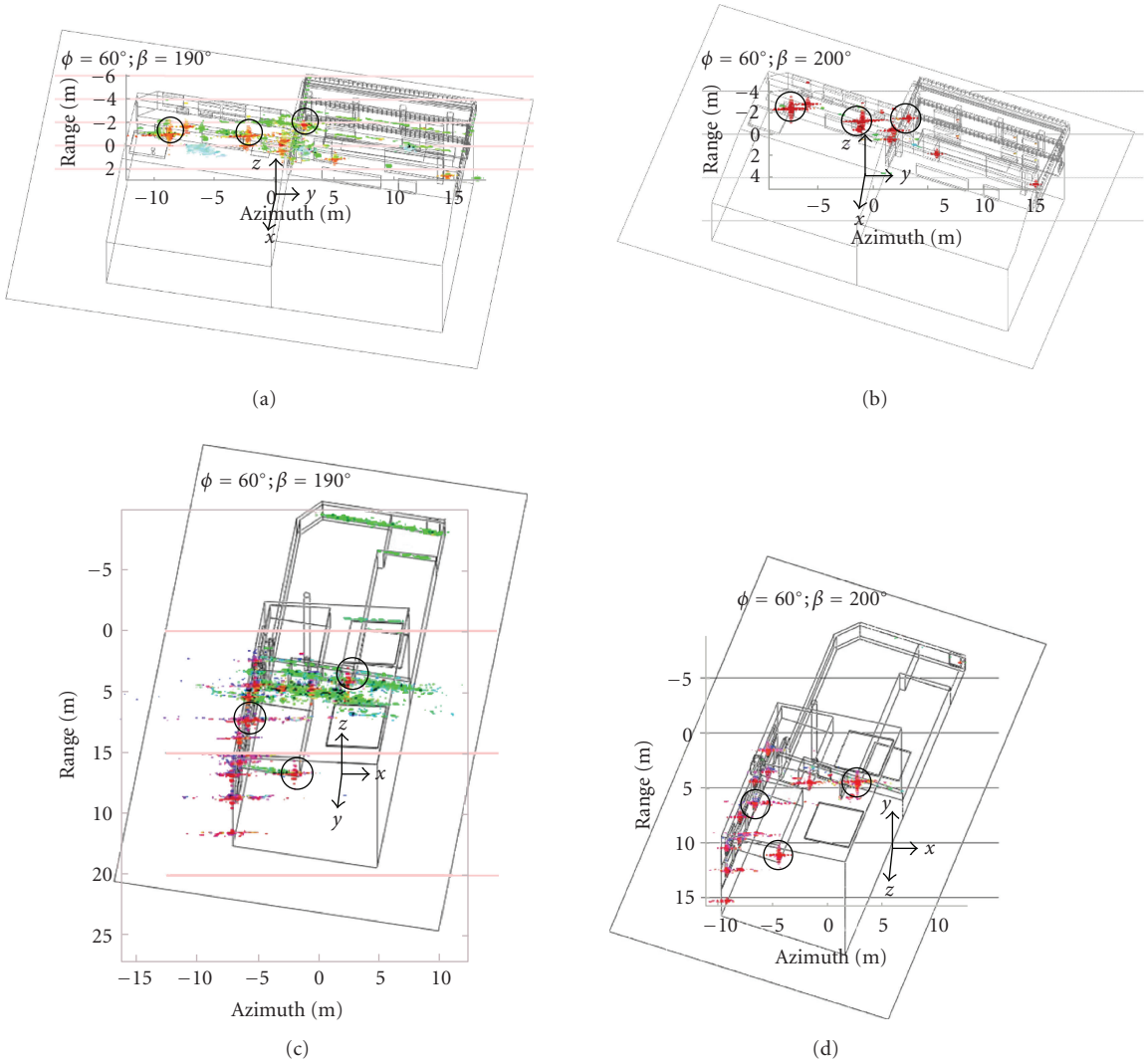

FIGURE 4: Scattering maps obtained for two building models at X band with $\beta \in \{190, 200\}^\circ$ and $\phi = 20^\circ$. They have been analyzed with the Pauli CTD theorem for a dynamic range of 25 dB. The models cover a maximum area of 50 square meters. Circles isolate the PePSs used in the feature vectors of Table 2.

thinking in classification (according to previous scattering analysis), but in other applications, such as subsidence, monitoring via PolInSAR is performed. There, the isolation of a set of guide scatterers with stable scattering properties is essential to retrieve accurate estimations of terrain deformation velocities along slant-range. So, the higher the scattering characterization is, the better the confidence is achieved. In single polarimetric SAR, this technique is mature, and now it is being successfully exploited in real scenarios [35, 36]. However, it has not migrated yet to PolInSAR, and so the current work would be helpful.

In contrast to the case with ships, SAR simulations are presented in terms of a 3D scattering map, where the relative scatter height is displayed jointly with the value of $|p^j_{n,xx}|$ (the previous RGB color code is also adopted here). These maps are shown in Figure 6 ($\phi = 60^\circ$, $\beta = 190^\circ$) and allow the isolation of almost all the PePSs identified in Section 3.2 with a confidence of ~75%. With these maps, a type of product similar to the ISAR one, but with less sensor requirements, can be obtained for scattering analysis [7]. One main advantage is the possibility to isolate different scatterers within the same resolution cell. This is advanced in Section 2.2 and related to the increased discrimination capability supplied by polarimetric channels. This permits to increase the accuracy in subsidence measurements due to the subpixel resolution that may be reached in some cells (in fact, those having PePSs, which can be considered as good candidates for use as subsidence guide scatterers).

5. MODEL EXPLOITATION

Once it has been shown that the proposed model of complex targets can be feasibly inverted in SAR images, the exploration of what applications can benefit is useful. In the case of ships, the application of this model can be considered mature, from which the novel VCA method resulted [7]. For

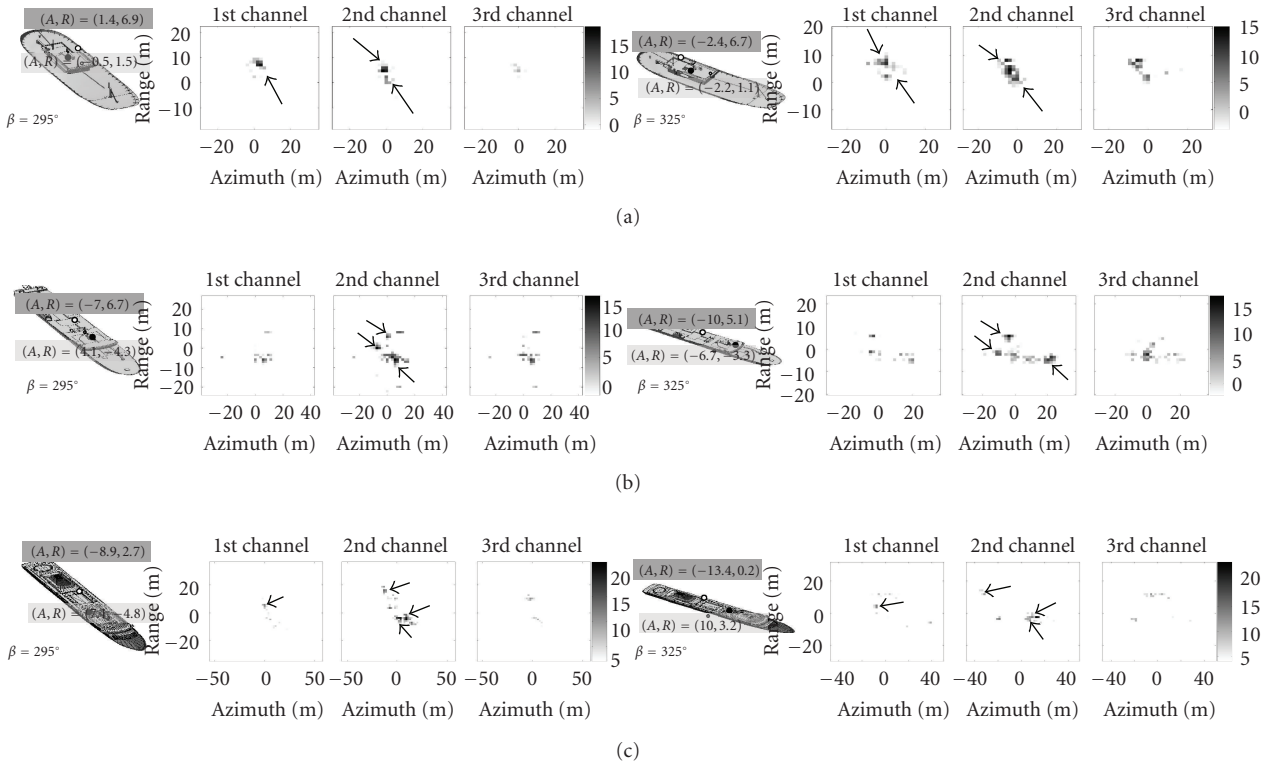

FIGURE 5: Pauli gray images showing the weight of each Pauli channel for the X band PolInSAR simulations of ships. The targets are $j = S0$ (a), $j = S1$ (b), and $j = S2$ (c) taking the bearing values of $\beta = 295, 325^\circ$. The arrows locate the reference PePSs gathered in the feature vectors of Table 1, where positions are transformed into the SAR azimuth slant-range grid according to the user incidence and bearing angles.

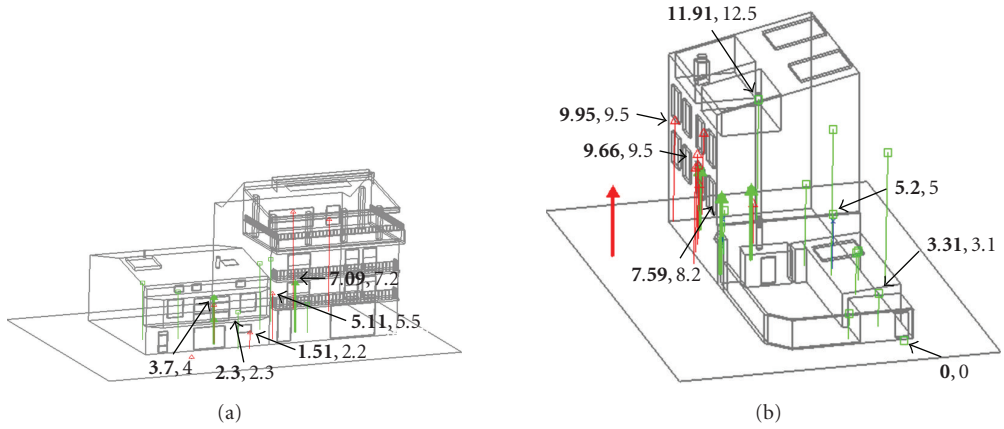

FIGURE 6: 3D scattering maps retrieved with PolInSAR for urban simulations ($\phi = 60^\circ$, $\beta = 190^\circ$). Bold and normal numbers indicate measured and expected heights for the highlighted scatterers. Model and data coregistration is made with a set of reference model points and imaging geometry.

urban targets, the study is in a preliminary stage and some guidelines for specific applications can be only provided.

5.1. Ship targets: VCA algorithm

The operating principle of VCA lies in analyzing the input PolInSAR dataset with the quad-pol Pauli vector (due to the fact that Pauli decomposition is a complete representation, the same simple mechanisms are isolated in any basis, e.g., linear or circular). This leads to three different interferograms (one per each Pauli mechanism), from which local maxima are isolated. All of them are combined in all possible permutations building estimated feature vectors with different lengths. These vectors are then correlated with the reference ones associated with specific ships, whose relative distance is quantified by a similarity parameter, S,

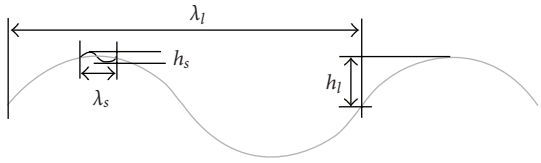

Figure 7: Scheme of the two-scale sea surface model.

Table 3: Scenario configurations for simulations in Section 4. Sea parameters are $h_l = 1.5$ m, $h_s = 0.1$ m, $\lambda_l = 100$ m, $\lambda_s = \lambda/(2\sin\phi)$.

Scenario	Bearings	Motions	Sea surface
0	$[295 : 10 : 355]^\circ$	No	No
1	$[295 : 10 : 355]^\circ$	Table 4	No
2	$[295 : 10 : 355]^\circ$	No	Two-scale
3	$[295 : 10 : 355]^\circ$	Table 4	Two-scale

Table 4: Rotational motions in the scenarios defined in Table 3. First-order angular velocities are expressed in rad/s.

β	$\dot{\delta}_{\text{roll}}$	$\dot{\delta}_{\text{pitch}}$	β	$\dot{\delta}_{\text{roll}}$	$\dot{\delta}_{\text{pitch}}$
295	−1.56	−0.26	335	−0.98	−1.16
305	−1.43	−0.52	345	−0.76	−1.32
315	−1.32	−0.76	355	−0.52	−1.43
325	−1.16	−0.98	—	—	—

based on an Euclidean norm [7]. The result is a quantitative manner for identifying the imaged ship with one of those within the available pattern base.

VCA performance is evaluated with a set of simulations similar to those of Figure 5. The same X band sensor has been used for a perpendicular baseline of $B^\perp = 30$ m and $\phi = 20^\circ$, and a resolution of 2.3 m in azimuth and 1.3 m in range [7]. The scenario considers the three types of ships for bearings ranging from 295 to 355 in steps of 10 degrees, surrounded by sea surface and experimenting ship motions. On the one hand, sea clutter is modeled with a two-scale approach for which a specific height profile is applied to the points of a dielectric discrete surface [17, 37–39]. The adopted complex dielectric permittivity is $\epsilon = 75 - j\cdot 27$, which corresponds to sea water with salinity of 35 psu and temperature of 25C [40, 41]. On the other hand, rotational and translational motions during image acquisition are considered by rotating the CAD model at each azimuth position. In real scenarios, ship motions can lead to important image distortions that are characterized by azimuth shifts. They normally cause notable geolocation errors and signature shape distortions [9, 42]. All environmental conditions are summarized in Tables 3 and 4. Sea main parameters are described in Figure 7, and pitching and rolling angular velocities are defined counterclockwise with respect to the rotation axis [9]. In all cases, ocean waves travel parallel to the ship from stern to bow.

Table 5 shows the similarity table for the specified bearings (the remaining ones provide similar results). They gather the similarity values related to each feature vector

Table 5: VCA similarity values, $0 < S < 1$, retrieved for the X band PolInSAR simulations with sea and ship motions.

$\beta = 295^\circ \mid \beta = 315^\circ$	SPA_{pat}	ICE_{pat}	FER_{pat}
Processing SPA	**0.57**|**0.44**	0.15|0	0|0.25
Processing ICE	0.1|**0.7**	**0.8**|0.44	0.1|0.25
Processing FER	0.21|0	0.3|0	**0.69**|**0.56**

when each ship is processed in the given observation conditions. As observed, all ships are well identified in almost all situations preserving a reasonable identification confidence against strong clutter. Two items are important: (1) the azimuth shifts help in some cases to improve the identification capability; (2) sea clutter appears to be the most adverse factor dropping the identification confidence. Specially adverse is for target $j = S1$whose lack of PePSs in the first Pauli channel makes the presence of the sea, with dominating sphere-like behaviors, increase the confusion with respect to the remaining ships. In general terms, VCA appears to be reliable enough as to consider its application in real scenarios. Further simulation studies give confidence to these asseveration and future measurement campaigns, which should try to provide the required framework for making the proper tests.

5.2. Urban targets: data interpretation

Section 4.2 has shown that the proposed model of complex targets may be useful for complementing single-pol subsidence studies, and may help in their possible migration to PolSAR systems (rather than developing classification). In this sense, the main advantage is the possibility to predict for which situations and geometries PePSs can be observed and considered as reliable guide scatterers for deformation studies.

Historically, urban applications have been related to orbital monitoring, because the velocity of changes can be assumed by the revisiting time of satellites, and historical databases for almost the same imaging geometry can be built. As a result, most geometries are expected to be imaged for a specific set of well-defined observation parameters and, hence, target model can be defined in urban environments as in ships. The only consideration is that feature vectors should meet the imaging geometries of current sensors rather than being expressed in terms of solid or radar aspect angles. In this context, feature vectors take sense, which may help, for example, to predict where the guide scatterers may be located. Such result would give a complementary reliability estimation of subsidence measurements, as well as refining and making the searching criteria more efficient.

6. CONCLUSION

This paper has presented a new modeling methodology for the SAR signatures of complex targets. The analysis of stacks of simulated images related to diversified scenarios, sensors, and types of targets is used to look for certain

reference scatterers (PePSs). Such scatterers accomplish a set of conditions focused to assure the discrimination among different types of geometries. Their 3D position and polarimetric scattering mechanism conform the bases of the model feature vectors, which allows to link the reflectivity information of SAR images with the macroscale structure of targets.

One of the main advantages of the proposed modeling approach is the minimization of the amount of real images required for testing the model. Certainly, simulated images can allow, in a first stage, the generation of preliminary version of models with reduced costs. Following this, these results would be used to define adequate measurement campaigns and model tests, which can lead to more refined solutions. In the current work, the first step has been tackled with the SAR simulator GRECOSAR, which has appeared to be an efficient tool for such scattering analysis.

GRECOSAR has been used to generate scattering maps for three types of ships and two types of buildings. The images have shown that PePS isolation is possible, but with different scattering sensitivity in both types of targets. While the same feature vector is valid for ships along a large set of observation conditions, buildings have to be identified with different vectors. The reason is their higher structure complexity and lack of symmetry.

The analysis of these results in SAR images has confirmed that the current model can be useful for different applications. In the case of ships, classification techniques may benefit as target discrimination can be reached via a quantitative and robust manner. This has been shown by presenting the novel VCA method, which allows, according to tests performed in simulated scenarios, high identification ratios even against sea clutter and ship motions. In the past, these items have become important limitations for classical methods. For urban scenarios, the current model is useful for fixing structures which are potential candidates for use in subsidence applications. Improved interpretation of interferometric data is also an important item, which may benefit the development of height profiles or better real-data analysis.

Therefore, the scattering-based model seems viable for ships and urban-like targets. Its exploitation in SAR imagery needs, however, from PolInSAR sensors with recommended resolutions lower than 3 m so that PePSs can be properly isolated. In the case of ships, single-pass modes are very demanding as it is not clear whether satellite-based solutions could be someday available. On the contrary, just launched designs as TerraSAR-X and Radarsat-2 can provide repeat-pass capabilities useful for urban applications. Future works should devote efforts for evaluating the model in real images so that definitive confidence to the model and related applications can be reached.

ACKNOWLEDGMENTS

This work was supported by Spanish Ministerio de Educación y Ciencia (MEC) and EU Fondos Europeos para el Desarrollo Regional (FEDER) funds under Project no. TEC2005-06863-C02-01.

REFERENCES

[1] A. Roth and R. Werninghaus, "Status of the TerraSAR-X mission," in *Proceedings of the International Geoscience and Remote Sensing Symposium (IGARSS '06)*, pp. 1918–1920, Denver, Colo, USA, July-August 2006.

[2] R. Touzi, R. K. Raney, and F. Charbonneau, "On the use of permanent symmetric scatterers for ship characterization," *IEEE Transactions on Geoscience and Remote Sensing*, vol. 42, no. 10, pp. 2039–2045, 2004.

[3] S. Guillaso, L. Ferro-Famil, A. Reigber, and E. Pottier, "Building characterization using L-band polarimetric interferometric SAR data," *IEEE Geoscience and Remote Sensing Letters*, vol. 2, no. 3, pp. 347–351, 2005.

[4] R. Z. Schneider, K. P. Papathanassiou, I. Hajnsek, and A. Moreira, "Polarimetric and interferometric characterization of coherent scatterers in urban areas," *IEEE Transactions on Geoscience and Remote Sensing*, vol. 44, no. 4, pp. 971–983, 2006.

[5] D. Perissin and A. Ferretti, "Urban-target recognition by means of repeated spaceborne SAR images," *IEEE Transactions on Geoscience and Remote Sensing*, vol. 45, no. 12, pp. 4043–4058, 2007.

[6] G. Margarit, *Marine applications of SAR polarimetry*, Ph.D. dissertation, Remote Sensing Laboratory (RSLab), Universitat Politècnica de Catalunya, Barcelona, Spain, July 2007.

[7] G. Margarit, J. J. Mallorqui, and X. Fàbregas, "Single-pass polarimetrie SAR interferometry for vessel classification," *IEEE Transactions on Geoscience and Remote Sensing*, vol. 45, no. 11, pp. 3494–3502, 2007.

[8] G. Margarit, J. Mallorqui, I. Corney, L. Pipia, C. López, and F. X. Fàbregas, "Analysis of urban areas scattering with simulated SAR imagery," in *Proceedings of ESA Fringe Workshop*, Frascati, Italy, November 2007.

[9] G. Margarit, J. J. Mallorqui, J. M. Rius, and J. Sanz-Marcos, "On the usage of GRECOSAR, an orbital polarimetric SAR simulator of complex targets, to vessel classification studies," *IEEE Transactions on Geoscience and Remote Sensing*, vol. 44, no. 12, pp. 3517–3526, 2006.

[10] J. M. Rius, M. Ferrando, and L. Jofre, "High-frequency RCS of complex radar targets in real-time," *IEEE Transactions on Antennas and Propagation*, vol. 41, no. 9, pp. 1308–1319, 1993.

[11] J. M. Rius, M. Vall-llossera, and A. Cardama, "GRECO: graphical processing methods for high frequency RCS prediction," *Annals of Telecommunications*, vol. 50, no. 5-6, pp. 551–556, 1995.

[12] *IMPAST project final report with reference (IMPAST/D 1.4/2.0) and under contract nr: Q5RS-2001-02266*, IMPAST consortium, DG-FISH.

[13] *DECLIMS project*, Joint Research Center (JRC), European Comission, https://declims.jrc.ec.europa.eu/1.

[14] *Land and Sea Integrated Monitoring for European Security (LIMES) project*, European Comission, 6th Framework Programme.

[15] *GID*, Manual of; International Center for Numerical Methods in Engineering (CIMNE).

[16] G. Margarit, J. J. Mallorqui, C. López-Martínez, and J. Fortuny-Guasch, "Phenomenological vessel scattering study based on simulated inverse SAR imagery," submitted to *IEEE Transactions on Geoscience and Remote Sensing*.

[17] G. Margarit, J. J. Mallorqui, C. López-Martínez, and J. Fortuny-Guasch, "Exploitation of Ship Scattering in Polarimetric SAR for an Improved Classification under High Clutter

Conditions," accepted for publication at *IEEE Transactions of Geoscience and Remote Sensing*.

[18] R. Touzi and F. Charbonneau, "Characterization of target symmetric scattering using polarimetric SARs," *IEEE Transactions on Geoscience and Remote Sensing*, vol. 40, no. 11, pp. 2507–2516, 2002.

[19] S. R. Cloude and E. Pettier, "A review of target decomposition theorems in radar polarimetry," *IEEE Transactions on Geoscience and Remote Sensing*, vol. 34, no. 2, pp. 498–518, 1996.

[20] P. A. Rosen, S. Hensley, I. R. Joughin, et al., "Synthetic aperture radar interferometry," *Proceedings of the IEEE*, vol. 88, no. 3, pp. 333–382, 2000.

[21] W.-M. Boerner, S. R. Cloude, and E. Poitier, "Radar polarimetry and interferometry," Tech. Rep. RTO-EN-SET-081, NATO Research & Technology Organisation, Paris, France, 2004.

[22] W.-M. Boerner, L. A. Cram, W. A. Holm, et al., *Direct and Inverse Methods in Radar Polarimetry*, NATO ASI Series C: Mathematical and Physical Sciences, Kluwer Academic Publishers, Dordrecht, The Netherlands, 1985.

[23] R. K. Raney, "Dual-polarized SAR and stokes parameters," *IEEE Geoscience and Remote Sensing Letters*, vol. 3, no. 3, pp. 317–319, 2006.

[24] R. K. Raney, "Hybrid-polarity SAR architecture," *IEEE Transactions on Geoscience and Remote Sensing*, vol. 45, no. 11, pp. 3397–3404, 2007.

[25] J.-C. Souyris, P. Imbo, R. Fjørtoft, S. Mingot, and J.-S. Lee, "Compact polarimetry based on symmetry properties of geophysical media: the $\pi/4$ mode," *IEEE Transactions on Geoscience and Remote Sensing*, vol. 43, no. 3, pp. 634–645, 2005.

[26] M. Tello, C. López-Martínez, and J. J. Mallorqui, "A novel algorithm for ship detection in SAR imagery based on the wavelet transform," *IEEE Geoscience and Remote Sensing Letters*, vol. 2, no. 2, pp. 201–205, 2005.

[27] D. J. Crisp, "The state-of-the-art in ship detection in synthetic aperture radar imagery," Public Release Document DSTO-RR-0272, Defence Science and Technology Organization (DSTO), Department of Defence, Australian Government, Canberra, Australia, 2004.

[28] D. Perissin, C. Prati, and F. Rocca, "ASAR parallel-track PS analysis in urban sites," in *Proceedings of the International Geoscience and Remote Sensing Symposium (IGARSS '07)*, pp. 1167–1170, Barcelona, Spain, June 2007.

[29] F. Cao, W. Hong, Y. Wu, and E. Pottier, "An unsupervised segmentation with an adaptive number of clusters using the SPAN/H/α/A space and the complex Wishart clustering for fully polarimetrie SAR data analysis," *IEEE Transactions on Geoscience and Remote Sensing*, vol. 45, no. 11, pp. 3454–3467, 2007.

[30] S. N. Madsen, *Syntehtic Aperture Radar Interferometry: Principles and Applications*, Artech House, Boston, Mass, USA, 1999.

[31] S. Musman, D. Kerr, and C. Bachmann, "Automatic recognition of ISAR ship images," *IEEE Transactions on Aerospace and Electronic Systems*, vol. 32, no. 4, pp. 1392–1404, 1996.

[32] G. Zilman, A. Zapolski, and M. Marom, "The speed and beam of a ship from its wake's SAR images," *IEEE Transactions on Geoscience and Remote Sensing*, vol. 42, no. 10, pp. 2335–2343, 2004.

[33] L. Pipia, X. Fabregas, A. Aguasca, C. López-Martínez, J. J. Mallorqui, and O. Moraline, "Polarimetric temporal information for urban deformation map retrieval," in *Proceedings of the International Geoscience and Remote Sensing Symposium (IGARSS '07)*, pp. 192–195, Barcelona, Spain, June 2007.

[34] L. Pipia, X. Fàbregas, A. Aguasca, and C. López-Martínez, "Atmospheric artifact compensation in ground-based DInSAR applications," *IEEE Geoscience and Remote Sensing Letters*, vol. 5, no. 1, pp. 88–92, 2008.

[35] A. Ferretti, C. Prati, and F. Rocca, "Permanent scatterers in SAR interferometry," *IEEE Transactions on Geoscience and Remote Sensing*, vol. 39, no. 1, pp. 8–20, 2001.

[36] O. Mora, *Advanced differential interferometric SAR techniques for detection of terrain and building displacements*, Ph.D. dissertation, Remote Sensing Laboratory (RSLab), Universitat Politècnica de Catalunya, Barcelona, Spain, April 2004.

[37] W. J. Plant, W. C. Keller, and K. Hayes, "Measurement of river surface currents with coherent microwave systems," *IEEE Transactions on Geoscience and Remote Sensing*, vol. 43, no. 6, pp. 1242–1257, 2005.

[38] R. O. Harger, "A sea surface height estimator using synthetic aperture radar complex imagery," *IEEE Journal of Oceanic Engineering*, vol. 8, no. 2, pp. 71–78, 1983.

[39] G. Margarit and J. J. Mallorqui, "Discretization effects in sea surface simulation applied to ship classification studies," in *Proceedings of the 2nd International SAR Oceanography Workshop (SEASAR '08)*, Frascati, Italy, January 2008.

[40] V. Hesany, W. J. Plant, and W. C. Keller, "The normalized radar cross section of the sea at 10° incidence," *IEEE Transactions on Geoscience and Remote Sensing*, vol. 38, no. 1, pp. 64–72, 2000.

[41] S. Blanch and A. Aguasca, "Dielectric permittivity measurements of sea water at L band," in *Proceedings of the 1st Results Workshop on EuroSTARRS, WISE, LOSAC Campaigns*, pp. 137–141, Toulouse, France, November 2002.

[42] K. Ouchi, M. Iehara, K. Morimura, S. Kumano, and I. Takami, "Nonuniform azimuth image shift observed in the Radarsat images of ships in motion," *IEEE Transactions on Geoscience and Remote Sensing*, vol. 40, no. 10, pp. 2188–2195, 2002.